# Air Pollution
# ENV-409

## Transport of air pollution
## (abridged version)

# Atmospheric vertical structure

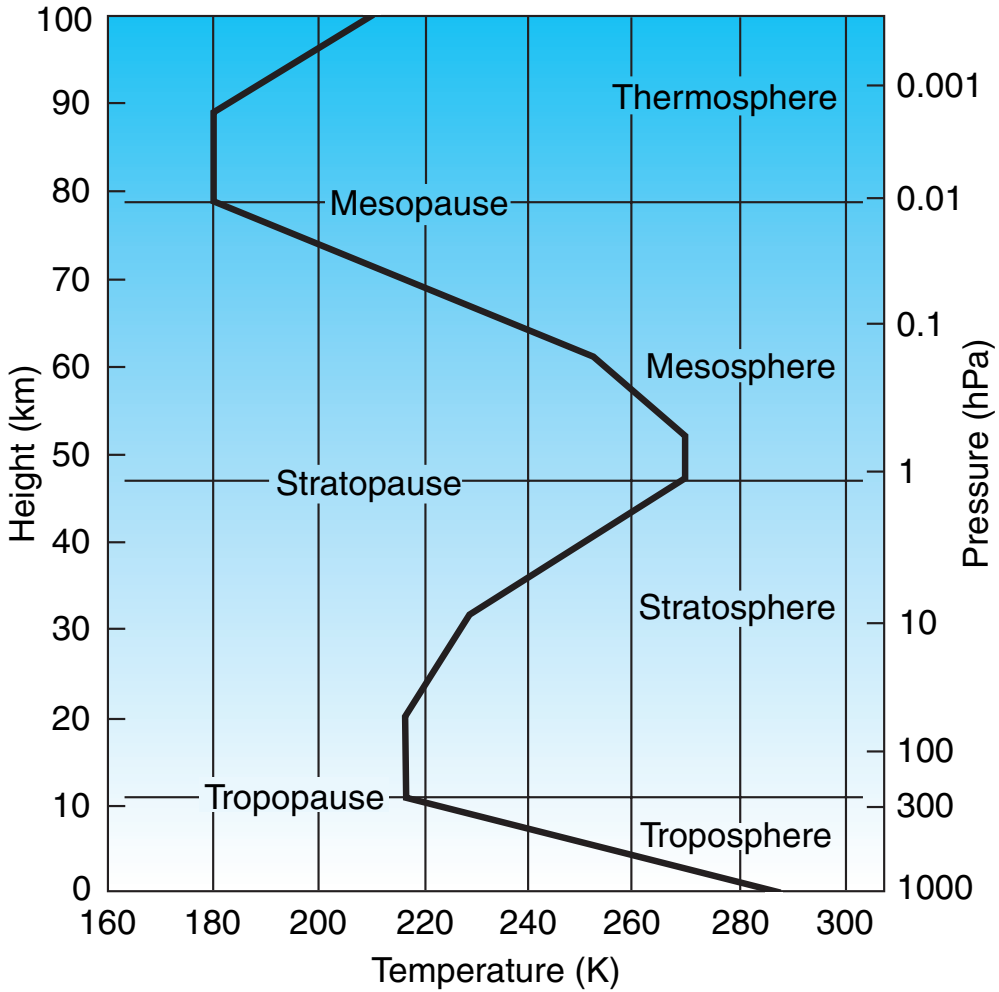


Wallace and Hobbs (2006)

# Lifetimes for atmospheric species

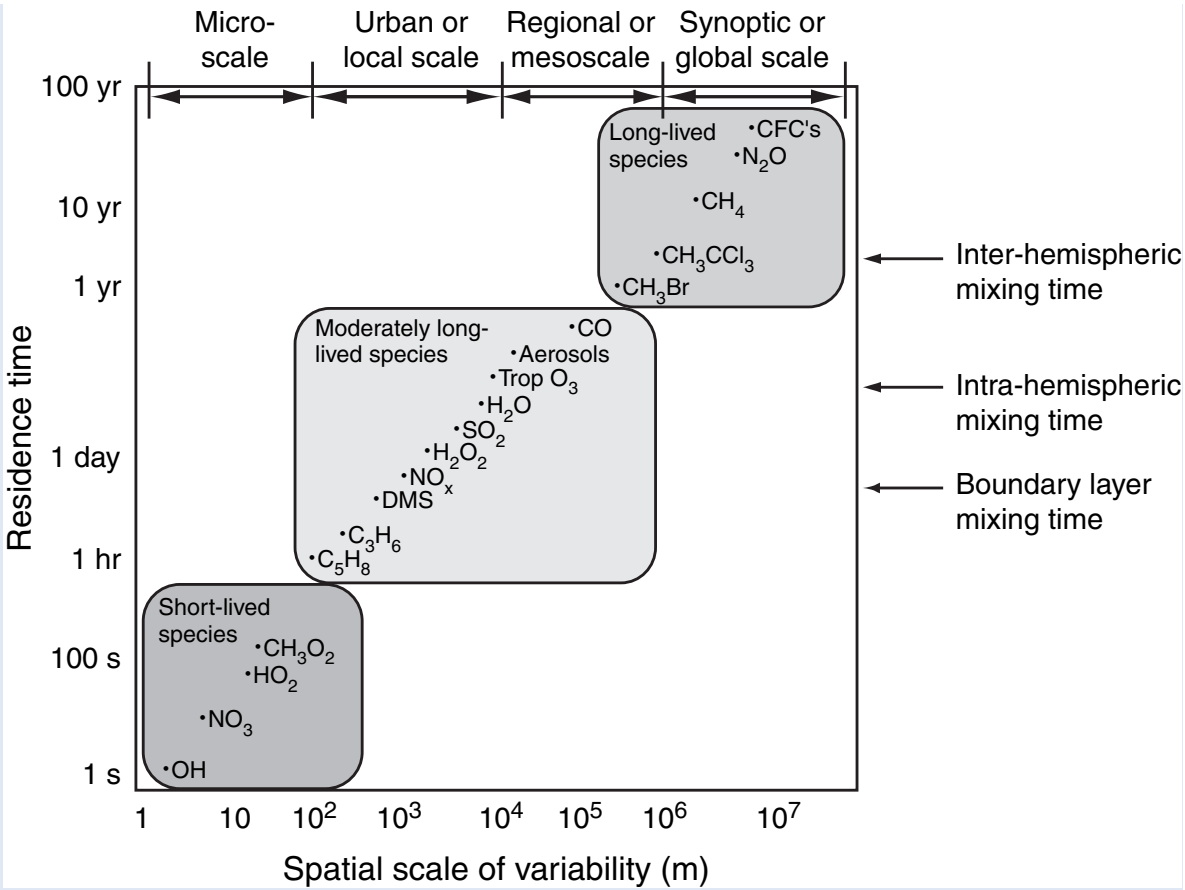


Wallace and Hobbs (2006)

Pollutants are removed by

- chemical transformation
- dry deposition
- wet deposition

# Timescales for vertical transport

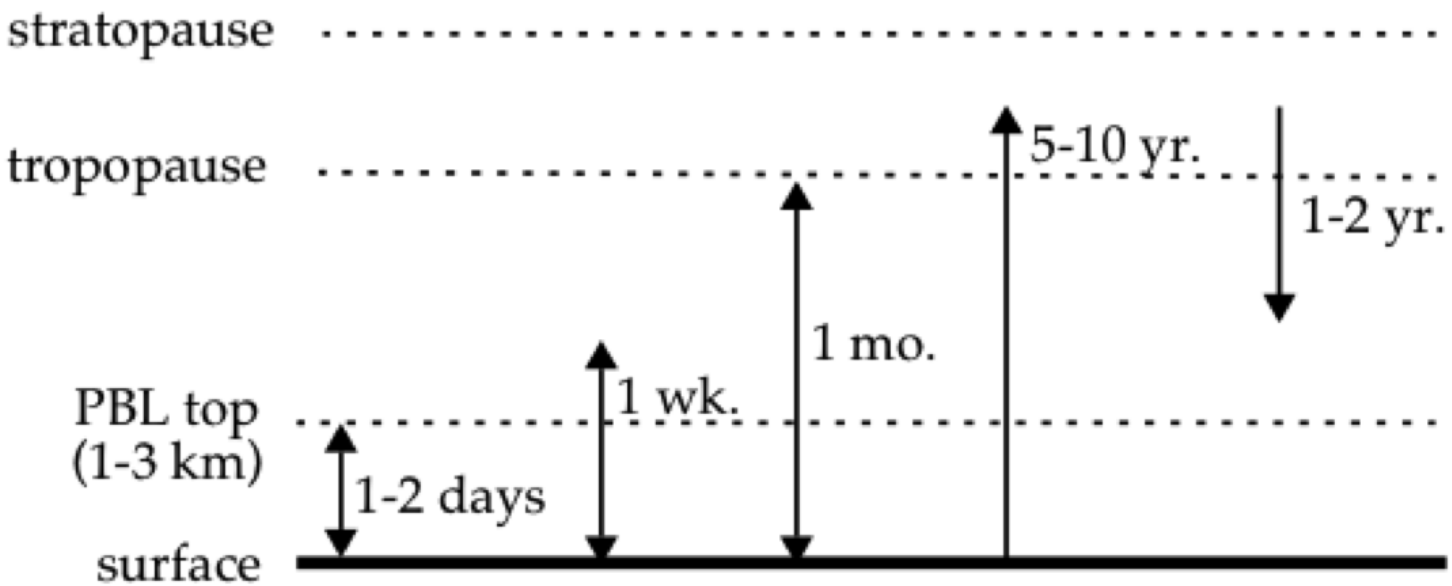


**Figure 4-24 Characteristic time scales for vertical transport**

Jacob (1999)

# Timescales for horizontal transport

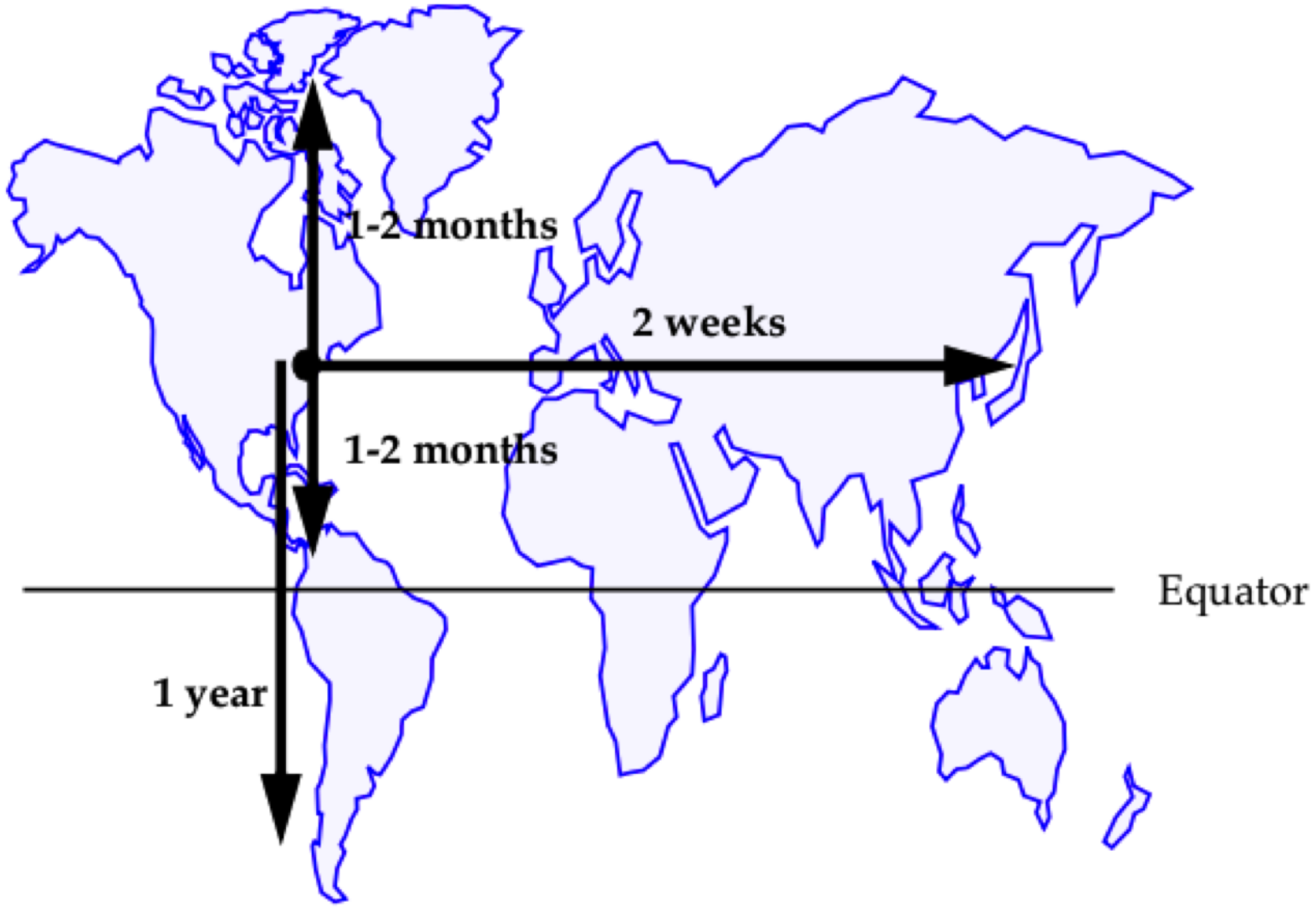


**Figure 4-12 Typical time scales for global horizontal transport in the troposphere**

Jacob (1999)

# How does atmospheric transport affect air pollution?

*Horizontal pollution transport*.

- Simple model of atmospheric general circulation
  - No rotation: uneven heating explains N-S circulation
  - Rotation explains Westerlies and trade winds
- Altitude-dependent flow regimes
  - Free troposphere
  - Within planetary boundary layer

*Vertical pollution transport*.

- Vertical convection (too slow to match observed transport times)
- Buoyant motion and turbulent mixing in the boundary layer

Principal forces

Real forces:

- pressure
- friction

Apparent forces arising from rotating frame of reference:

- centrifugal
- Coriolis

Wallace and Hobbs (2006)

# Apparent forces

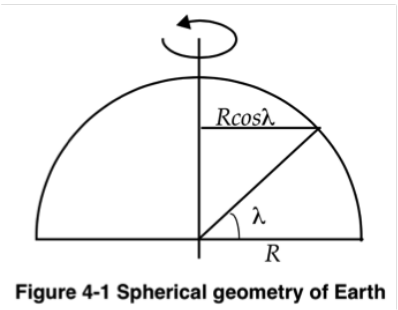


Figure 4-1 Spherical geometry of Earth

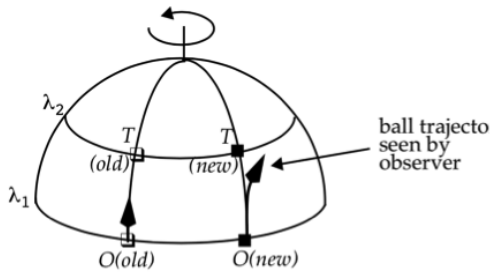


Figure 4-3 Coriolis effect for meridional motion

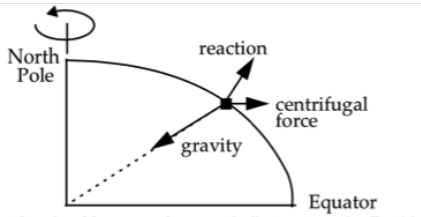


Figure 4-4 Equilibrium triangle of forces acting on a ball at rest on the Earth's surface. The non-sphericity of the Earth is greatly exaggerated.

Jacob (1999)

# Governing equations

Ideal gas law applied to air

$$\rho = \frac{M_{\text{air}} p}{RT} \tag{1}$$

Barometric equation (basic equation of fluid statics)

$$\frac{dp}{dz} = -\rho g \tag{2}$$

Reversible, adiabatic expansion (from thermodynamic cycle) given constant pressure heat capacity $C_p$:

$$\frac{dp}{p} = \frac{C_p}{R}\frac{dT}{T} \tag{3}$$

Continuity:

$$\frac{\partial \rho}{\partial t} + \nabla \cdot (\rho \mathbf{u}) = 0$$

Conservation of momentum for compressible fluid:

$$\frac{d\mathbf{u}}{dt} + 2\boldsymbol{\Omega} \times \mathbf{u} = -\frac{1}{\rho}\nabla p - \nabla \Phi + \mathbf{f}$$

where

- $2\boldsymbol{\Omega} \times \mathbf{u}$ is for the rotating frame of reference
- $\Phi$ is the geopotential

  $$\Phi = \int_{h=0}^{z} g(h)dh - \frac{1}{2}\Omega^2 r^2$$

  ($\nabla\Phi \approx \mathbf{g}$ for approximately constant $\mathbf{g}$).
- $\mathbf{f}$ embodies frictional forces due to viscous sheer:

  $$\mathbf{f} = \frac{\mu}{\rho}\nabla^2\mathbf{u} + \frac{1}{\rho}\left(\zeta + \frac{1}{3}\mu\right)\nabla(\nabla \cdot \mathbf{u})$$

  $\mu$ is the dynamic viscosity; $\zeta$ is the volume/bulk viscosity. For an incompressible fluid, $\nabla \cdot \mathbf{u} = 0$ and the last term in $\mathbf{f}$ vanishes. It is common to assume incompressible flow in various strata of the atmosphere (Boussinesq approximation).

# Flow regimes

Flow regimes:

- inviscid
- viscous
  - laminar
  - turbulent

Typical *Re* in the atmosphere is 1000–10,000 (turbulent $>$ 2000); this affects the equations of motion and dispersion of pollutants.

In the atmosphere, flow near the surface is influenced by surface roughness, and buoyancy motion induced by solar heating of the ground induces turbulence.

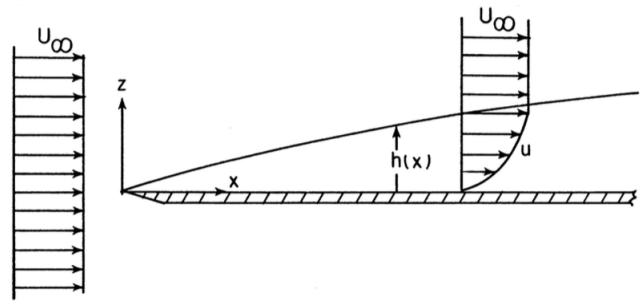


**Figure 7.4** Schematic of a developing boundary layer over a flat plate.

Arya (2001)

**Fig. 3.9** Visualization of a turbulent flow in the wind tunnel of Centrale Lyon (reproduction of the Bugey nuclear power plant). Credit: Centrale Lyon and French Institute of Nuclear Safety and Radiological Protection (Olivier Isnard)

Sportiisse (2010)

# Atmospheric vertical structure and flow regimes

The main atmospheric strata involved in pollutant transport.

The free troposphere/atmosphere extends from top of planetary boundary layer to the tropopause:

- *geostrophic flow* (inviscid, horizontal flow)

The planetary boundary layer (PBL) or atmospheric boundary layer (ABL):

- *Ekman layer* (extends from top of surface layer to $\sim$300–500 m): Balance of pressure, Coriolis, and friction forces. Wind direction changes as a function of height.
- *surface layer* (extends from surface to height of $\leq$ 30–50 m). Wind speed varies with height due to molecular exchange through turbulent eddies. This is where most pollutants are released.
- *laminar sublayer* (typically $<$ 1 cm). Important for deposition, but neglected for discussion on flow.

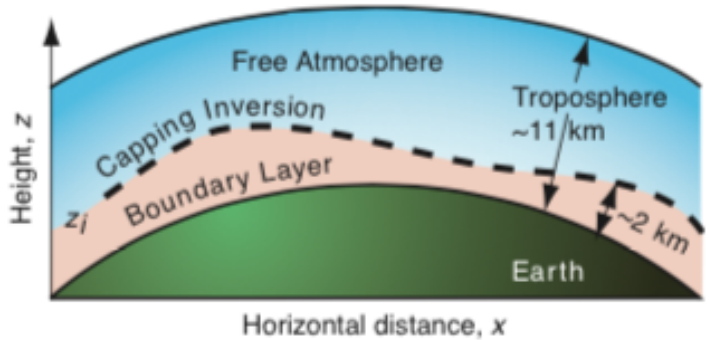


**Fig. 9.1** Vertical cross section of the Earth and troposphere showing the atmospheric boundary layer as the lowest portion of the troposphere. [Adapted from *Meteorology for Scientists and Engineers*, A Technical Companion Book to C. Donald Ahrens' Meteorology Today, 2nd Ed., by Stull, p. 65. Copyright 2000. Reprinted with permission of Brooks/Cole, a division of Thomson Learning: www.thomsonrights.com. Fax 800-730-22150.]

# Geostrophic flow

- At high altitudes, effect of surface can be neglected ( 500m)
- Balance of pressure-gradient and Coriolis forces

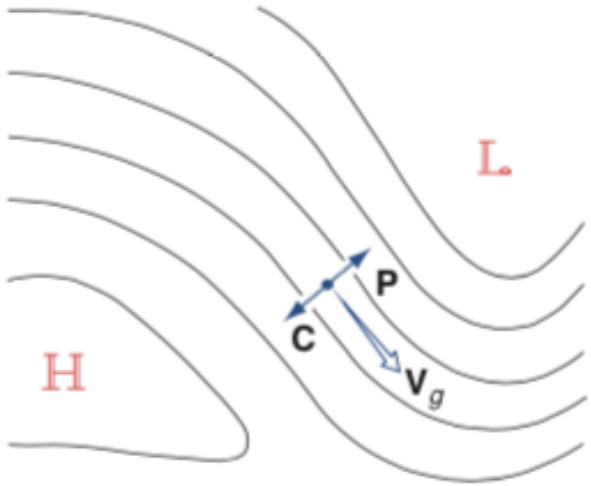


**Fig. 7.9** The geostrophic wind $V_g$ and its relationship to the horizontal pressure gradient force P and the Coriolis force C in the northern hemisphere.

# Intercontinental transport of pollutants

Species with lifetimes greater than transport times can influence air quality in other countries/continents. (Recall that species lifetimes are dependent on reactivity and removal rates by dry and wet deposition.)

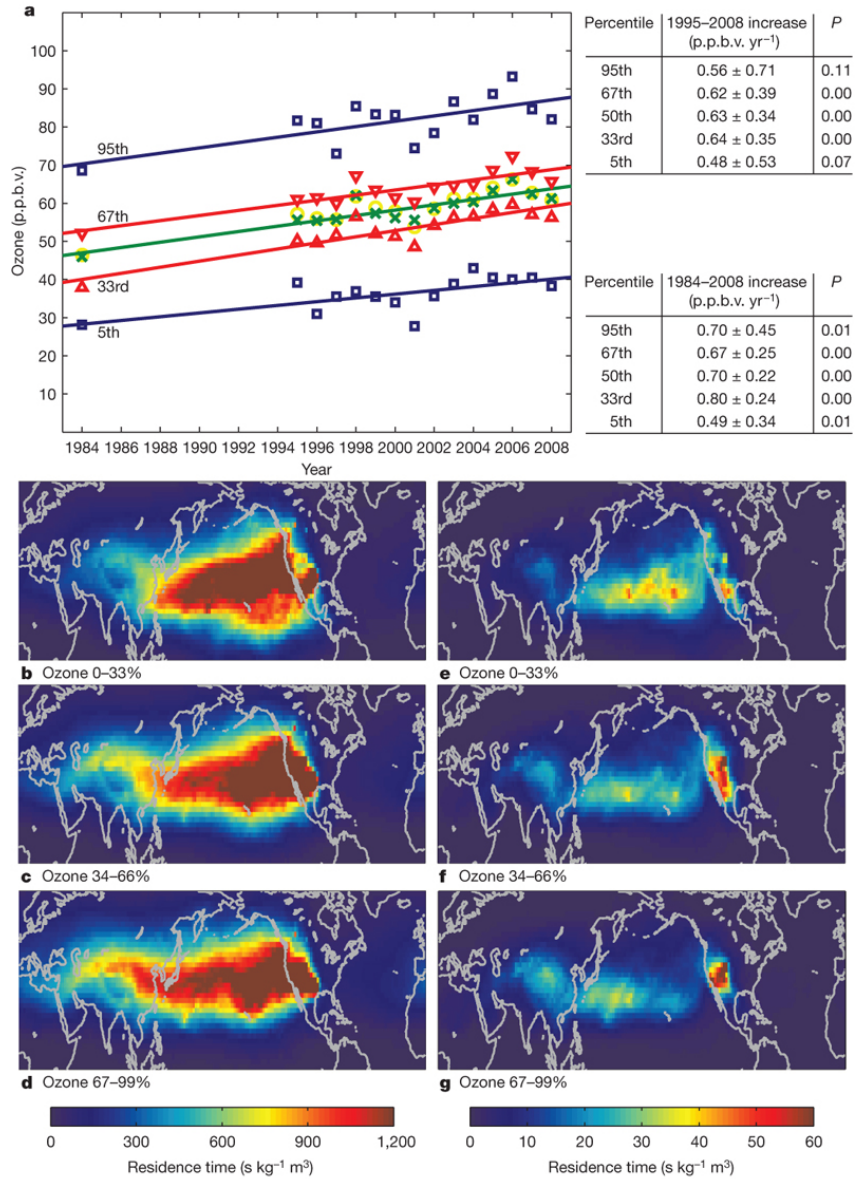


| Percentile | 1995–2008 increase (p.p.b.v. yr$^{-1}$) | P |
|---|---|---|
| 95th | 0.56 ± 0.71 | 0.11 |
| 67th | 0.62 ± 0.39 | 0.00 |
| 50th | 0.63 ± 0.34 | 0.00 |
| 33rd | 0.64 ± 0.35 | 0.00 |
| 5th | 0.48 ± 0.53 | 0.07 |

| Percentile | 1984–2008 increase (p.p.b.v. yr$^{-1}$) | P |
|---|---|---|
| 95th | 0.70 ± 0.45 | 0.01 |
| 67th | 0.67 ± 0.25 | 0.00 |
| 50th | 0.70 ± 0.22 | 0.00 |
| 33rd | 0.80 ± 0.24 | 0.00 |
| 5th | 0.49 ± 0.34 | 0.01 |

**Springtime ozone distributions for 1984, 1995–2008 in the mid-troposphere (3.0–8.0 km), and air mass source regions. a**, Distributions of springtime ozone measurements made in the troposphere between 3.0 and 8.0 km (stratospheric samples have been filtered out). The green line and data points are the median, and the yellow data points are means. The upper and lower blue lines (and data points) indicate the 95th and 5th percentiles. The upper and lower red lines (and data points) indicate the 67th and 33rd percentiles. Ozone sample sizes range from 1,663 in 1984 to 8,587 in 2006 [...]. Also shown are the ozone rates of increase for 1984–2008 and 1995–2008, as determined from the slope of the linear regression. The range on the slope indicates the 95% confidence limit that the slope lies within that range. **b–d**, The average 1984–2008 retroplume for three ranges of ozone measurements, expressed as column residence times. **e–g**, The corresponding retroplume residence times in the lowest 300 m of the atmosphere (the footprint layer). Ozone percentile ranges: **b** and **e**, 0–33rd, **c** and **f**, 34th–66th; **d** and **g**, 67th–99th. Column and footprint sample sizes are equal because every 15-day retroplume has some degree of transport through the lowest 300 m of the atmosphere.

Cooper et al. (2010)

# Horizontal windspeeds in the Ekman layer

Balance of pressure gradient, Coriolis, and frictional forces for an incompressible fluid. Solutions obtained assuming constant **K** near the surface turn out to be only qualitatively accurate, but shows that wind direction changes between surface and geostrophic flow.

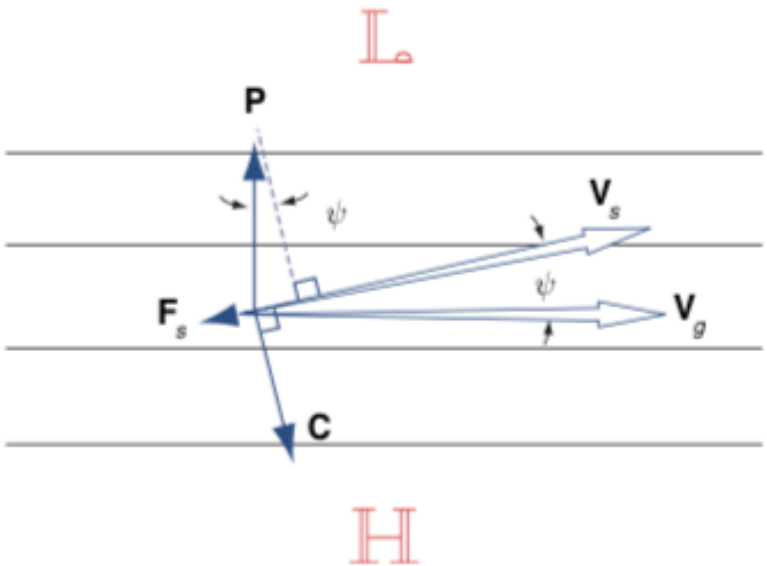


**Fig. 7.10** The three-way balance of forces required for steady surface winds in the presence of the frictional drag force F in the northern hemisphere. Solid lines represent isobars or geopotential height contours on a weather chart.

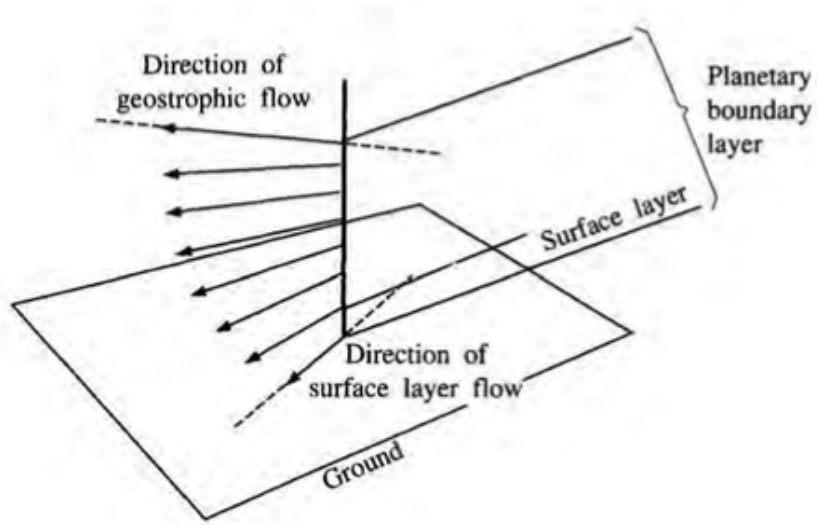


Seinfeld and Pandis (2006)

# Horizontal windspeeds in surface layer

The variation of wind with height in the surface layer is influenced by roughness (buildings, flora). The vertical velocity profile is not derived from first principles; but often parameterized as a power law relationship defined through a reference height $z_r$ and its corresponding velocity $u_r$:

$$u = u_r \left( \frac{z}{z_r} \right)^p$$

The exponent, $p$, is reported to vary between 0.07 to 0.60.

**TABLE 3-3** Value of Exponent, $p$, in Equation (3-13)

| Stability Category | Rural exponent | Urban Exponent |
|---|---|---|
| A | 0.07 | 0.15 |
| B | 0.07 | 0.15 |
| C | 0.10 | 0.20 |
| D | 0.15 | 0.25 |
| E | 0.35 | 0.30 |
| F | 0.55 | 0.30 |

Source: User's Guide for the ISC3 Dispersion Models, Vol. II, EPA-454/B-95-003b, U.S. EPA, September, 1995. Available on TTNWeb SCRAM.

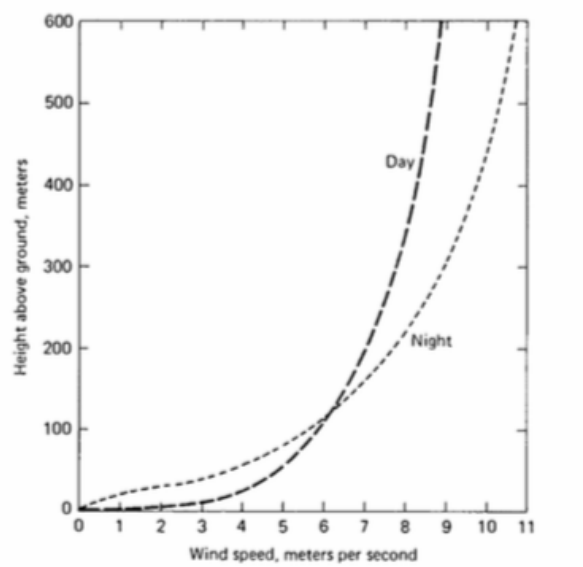


**FIGURE 3-12** Change of wind-speed profile with stability. (Source: D.B. Turner, *Workbook for Atmospheric Dispersion Estimates*. Washington, D.C.: HEW, 1969.)

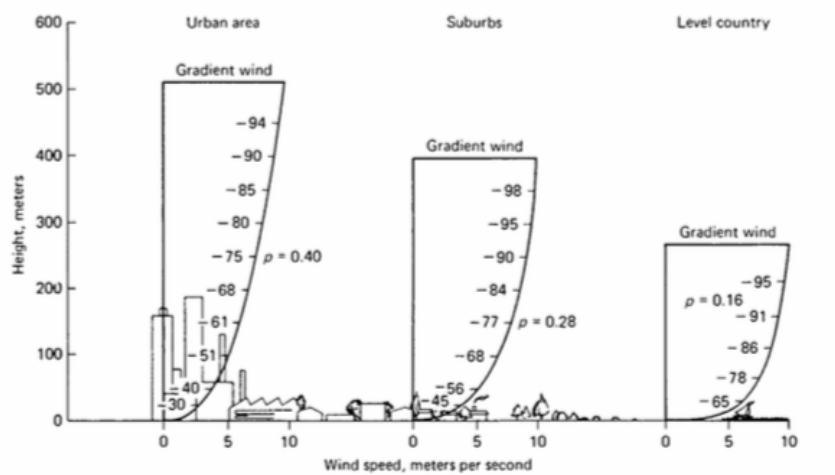


**FIGURE 3-13** Effect of terrain roughness on the wind-speed profile. Values along curves represent percentages of gradient wind value. (Source: D.B. Turner, *Workbook for Atmospheric Estimates*. Washington, D.C.: HEW, 1969.)

Wark et al. (1998)

# Maximum mixing depth (MMD)

- Thermal buoyancy effects determine the depth of the (convective) mixing layer.
- Greater the extent of mixing depth, larger the dilution volume.
- Definition:
  - vertical temperature profile of atmosphere for several km above earth's surface determined by balloon measurements (radiosonde)
  - compare against reference temperature profile obtained by heating air parcel from a ground-level temperature $T_0$ to a "maximum" $T_0'$ (hence "maximum" mixing depth) and expanded upward according to dry adiabatic lapse rate
  - the height at which the actual and reference temperature profiles intersect (density is same) is taken to be the MMD
- Typical values:
  - severe night inversion: $\sim$0 km
  - up to 2–3 km during daytime
  - higher values in afternoons (MMD - *maximum*) and lower values in mornings
- Higher likelihood of urban air pollution when MMD $<$1.5 km (common in many urban areas)

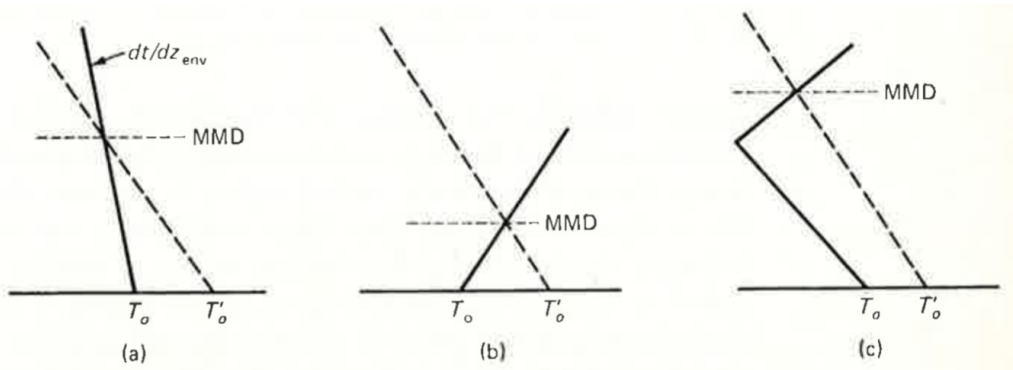


**FIGURE 3-14** Establishment of the maximum mixing depth (MMD) under various atmospheric conditions (adiabatic profile - - -, environmental profile—).

Wark et al. (1998)

# Inversion events

When the temperature increases with altitude, an *inversion* occurs → reduces vertical dispersion of pollutants, increases local concentrations.

- *subsidence inversion* — downward flow of air in a high-pressure region
  - high above emission sources (does not elevate pollutant concentrations in the short-term)
  - can persist for several days and contribute to long-term accumulation of pollutants
- *radiation inversion* — radiation from the earth's surface lost to the local atmosphere during nighttime
  - common phenomena
  - due to loss of radiation, ground surface quickly cools to temperatures below that of air at higher elevations

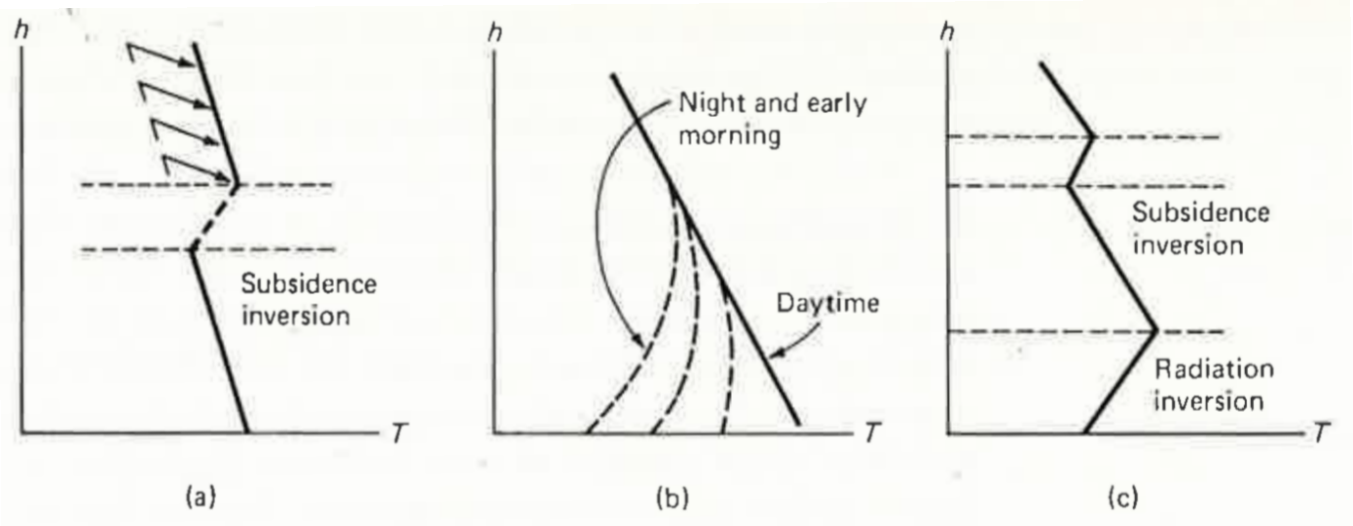


**FIGURE 3-10** Illustrations of (a) subsidence inversion, (b) radiation inversion, and (c) combination of subsidence and radiation inversions.

Wark et al. (1998)

# Diurnal growth of the PBL

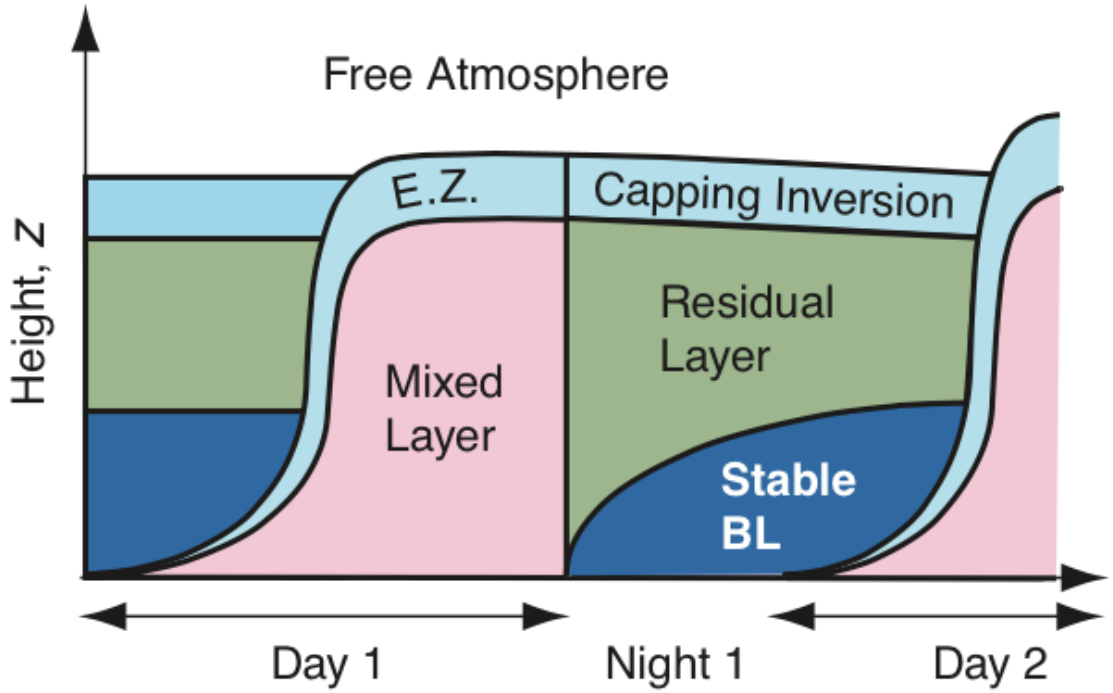


**Fig. 9.21** Vertical cross section of boundary-layer structure and its typical evolution during summer over land under fair-weather, cloud-free conditions. E.Z. indicates the entrainment zone. [Adapted from *Meteorology for Scientists and Engineers*, A Technical Companion Book to C. Donald Ahrens' Meteorology Today, 2nd Ed., by Stull, p. 69. Copyright 2000. Reprinted with permission of Brooks/Cole, a division of Thomson Learning: www.thomsonrights.com. Fax 800-730-2215.]

# Dispersion near roadways

- For simpler topologies, we can extend the point-source Gaussian plume model to model dispersion from a *line source*.
- For more complicated geometries (e.g., *urban canyons*), more complex models involving CFD might be used to resolve scales relevant for dispersion.
- Rate of dispersion is dependent on the pollutant and environmental conditions.

# Dispersion near roadways

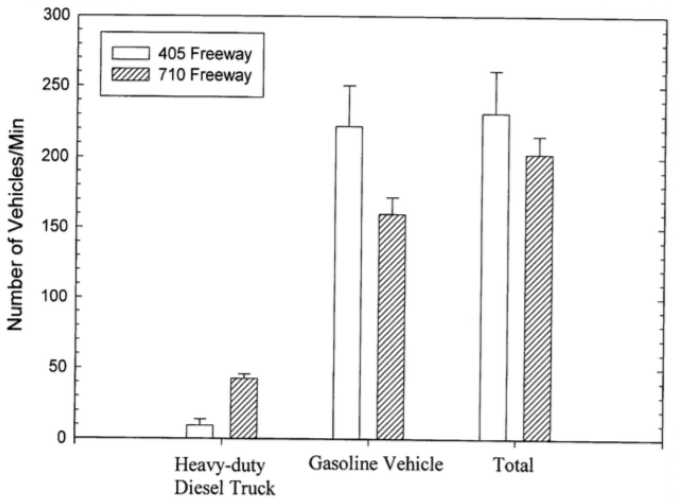


Zhu et al., *Atmos. Environ.* (2002)

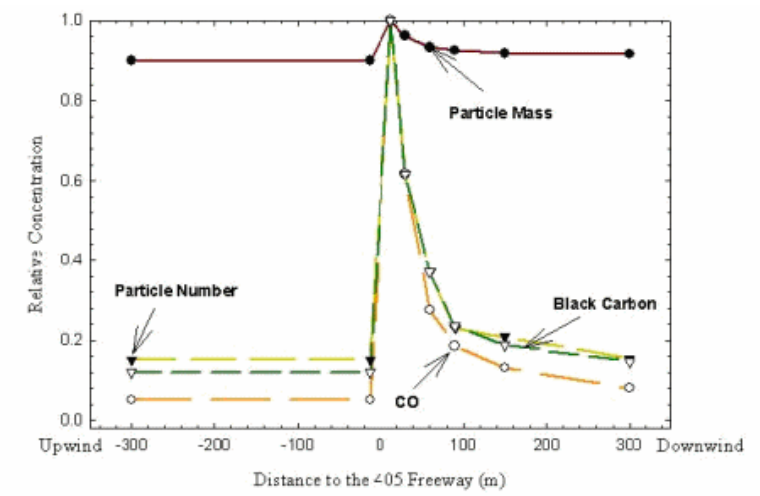


Zhu et al., *JAWMA* (2002)

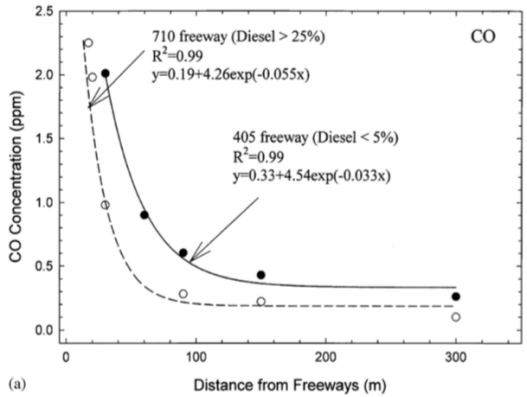


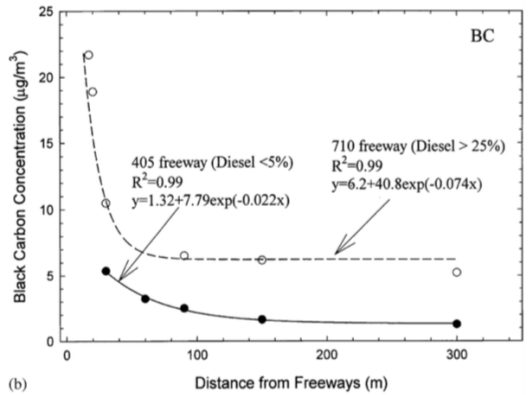


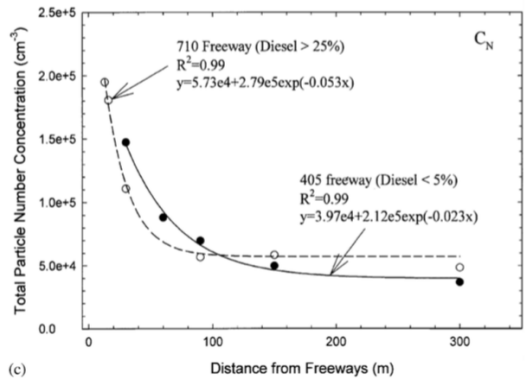


Zhu et al., *Atmos. Environ.* (2002)

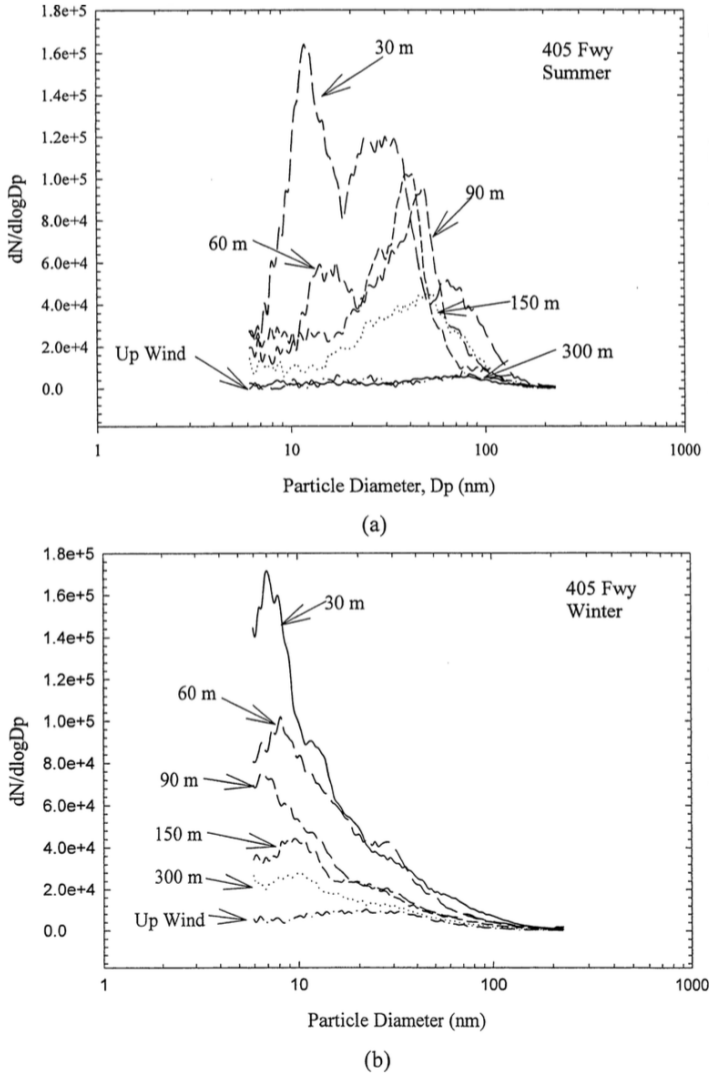


**Figure 2.** Ultrafine particle size distribution at different sampling locations near the 405 freeway in (a) summer and (b) winter.

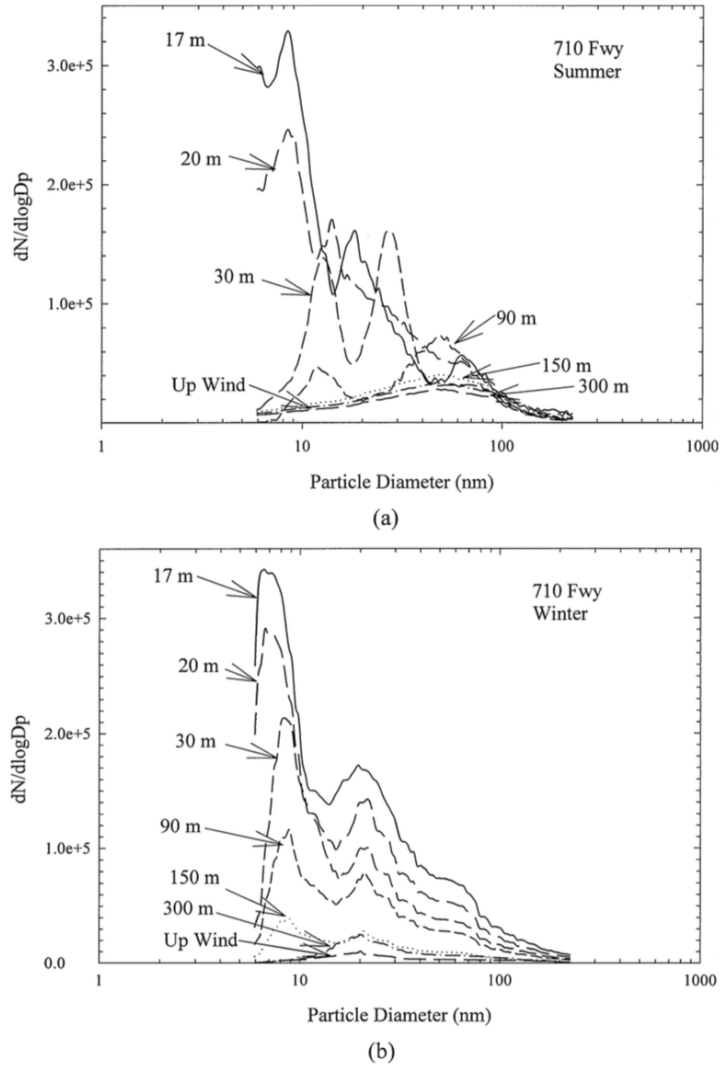


**Figure 3.** Ultrafine particle size distribution at different sampling locations near the 710 freeway in (a) summer and (b) winter.

Zhu et al., *Aerosol Sci. Tech.* (2004)

# Identifying source regions

- Wind direction
- Back trajectory analysis
- Statistical analysis

# Back-trajectory analysis with HYSPLIT

Based on meteorological data reanalysis that provides the velocity field $\boldsymbol{v}$, the advection of a "particle" (airmass) is computed from the average velocity at initial/current and first-guess positions $\overline{\boldsymbol{r}}(t)$ and $\overline{\boldsymbol{r}}^*(t+\Delta t)$, respectively.

$$\overline{\boldsymbol{r}}(t+\Delta t) = \overline{\boldsymbol{r}}(t) + 0.5\left[\boldsymbol{v}(\overline{\boldsymbol{r}}, t) + \boldsymbol{v}(\overline{\boldsymbol{r}}', t+\Delta t)\right]\Delta t$$
$$\overline{\boldsymbol{r}}^*(t+\Delta t) = \overline{\boldsymbol{r}}(t) + \boldsymbol{v}(\overline{\boldsymbol{r}}, t)\Delta t$$

A dispersion component can be added afterward:

$$r_x = \overline{r}_x(t+\Delta t) + v_x'(t+\Delta t)\Delta t$$
$$r_z = \overline{r}_z(t+\Delta t) + v_z'(t+\Delta t)\Delta t$$

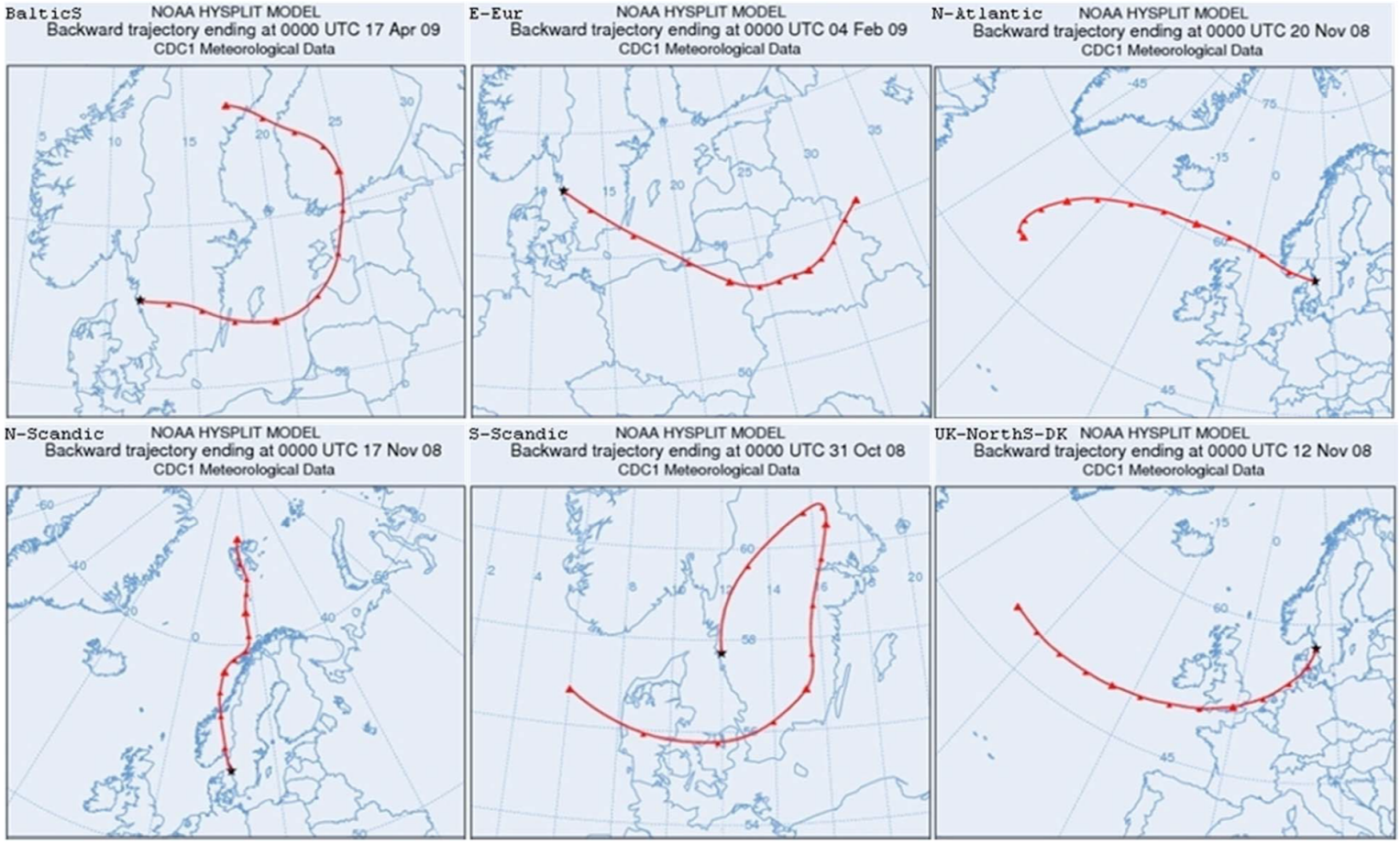


Molnár et al., *Environ. Sci.: Processes Impacts*, 2017

# Accounting for trajectory error

https://ready.arl.noaa.gov

How to examine trajectory errors (manual/conventional approach):

- Perturb starting location.
- Observe divergence of trajectories.

HYSPLIT ensemble approach:

- Compute trajectories about a 3-dimensional cube centered about the starting point.
- However, offset the meteorological data point associated with each trajectory so that all trajectories start from (or end at) the same point.

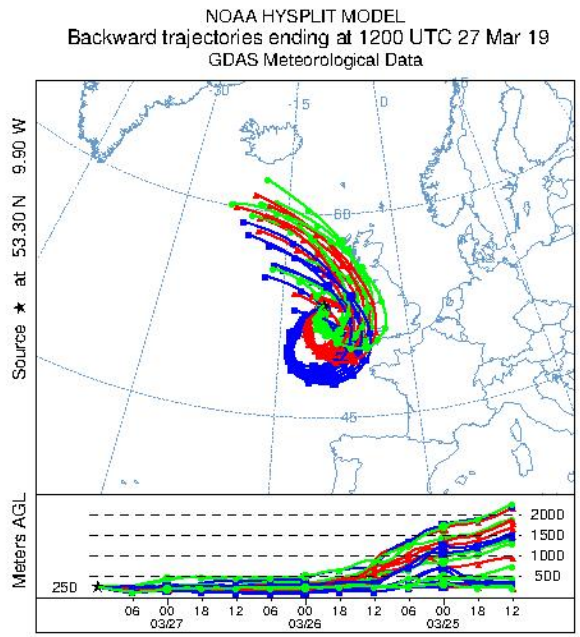


27 trajectories ending at noon at 250 m height

http://macehead.nuigalway.ie/rt/hysplit.html

# A few statistical approaches

Ashbaugh et al., *Atmos. Environ.*, 1985; P. Hopke and coworkers

Conditional probability function (CPF):

$$\mathrm{CPF}_{\Delta\theta} = \frac{m_{\Delta\theta}}{n_{\Delta\theta}}$$

---

Potential source contribution function (PSCF):

$$P(A_{ij}) = \frac{n_{ij}}{N} \quad \text{total trajectories}$$

$$P(B_{ij}) = \frac{m_{ij}}{N} \quad \text{high concentration}$$

$$\mathrm{PSCF}_{ij} = P(B_{ij}|A_{ij}) = \frac{m_{ij}}{n_{ij}} = \frac{\sum_{\ell\in\{high\}} \tau_{ij}^{\ell}}{\sum_{\ell\in\{total\}} \tau_{ij}^{\ell}}$$

Concentration field (CF) or concentration weighted trajectory (CWT) analysis:

$$\mathrm{CF}_{ij} = \frac{\sum_{\ell\in\{total\}} \log C_{ij}\tau_{ij}^{\ell}}{\sum_{\ell\in\{total\}} \tau_{ij}^{\ell}}$$

# CPF example

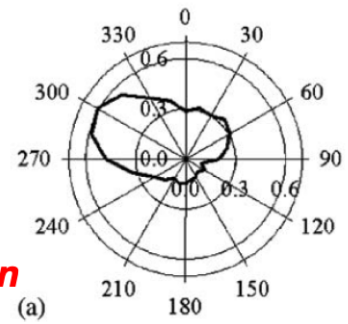


**oil combustion**

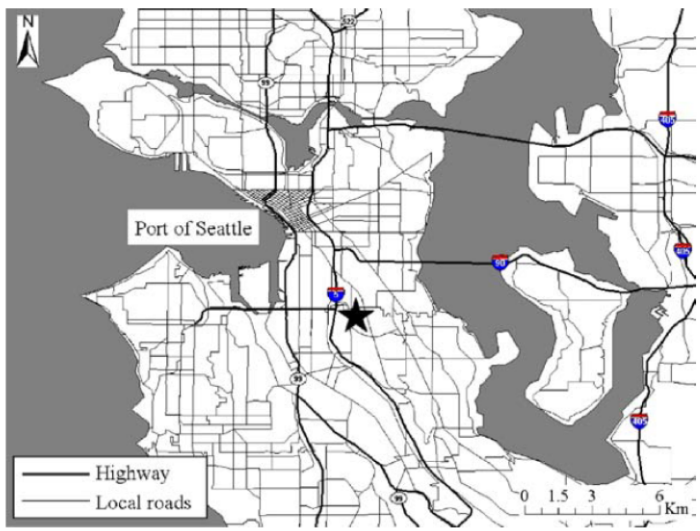


Fig. 1. Location of the monitoring site in Seattle, WA. The Beacon Hill monitoring site in Seattle is denoted by ★.

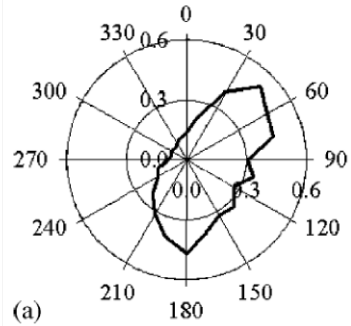


**sea salt**

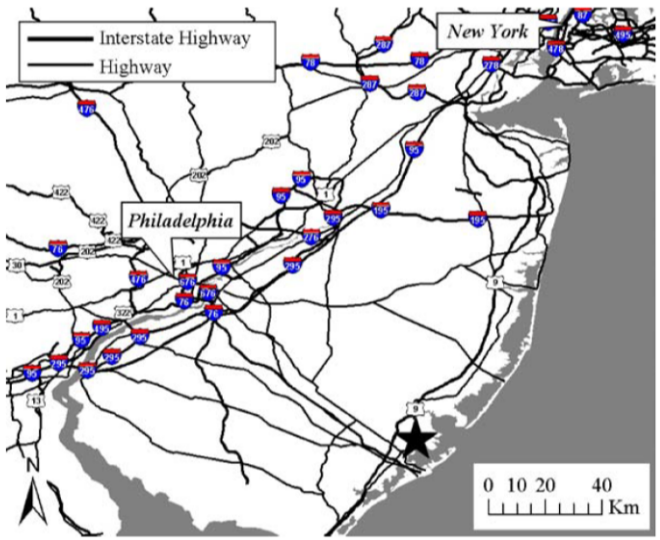


Fig. 3. Location of the monitoring site in Brigantine, NJ. The monitoring site is denoted by ★.

Kim and Hopke, *Atmos. Environ.*, 2004

# PSCF illustration

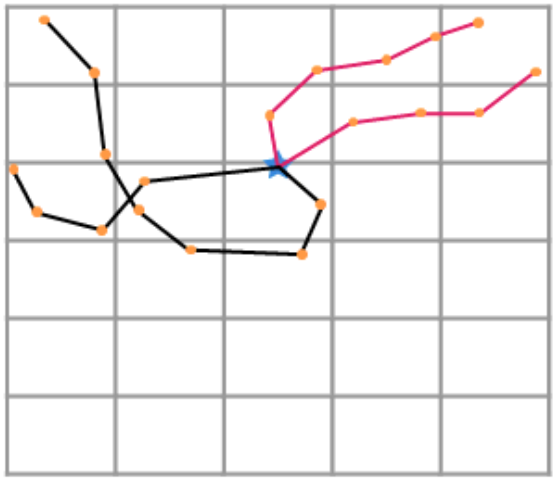

Receptor site

endpoint

traj. associated with high [ ]

matrix n

| | | | | |
|---|---|---|---|---|
| 2 | 0 | 1 | 2 | 2 |
| 1 | 0 | 1 | 2 | 1 |
| 2 | 2 | 5 | 0 | 0 |
| 0 | 1 | 1 | 0 | 0 |
| 0 | 0 | 0 | 0 | 0 |
| 0 | 0 | 0 | 0 | 0 |

matrix m

| | | | | |
|---|---|---|---|---|
| 0 | 0 | 1 | 2 | 2 |
| 0 | 0 | 1 | 2 | 1 |
| 0 | 0 | 2 | 0 | 0 |
| 0 | 0 | 0 | 0 | 0 |
| 0 | 0 | 0 | 0 | 0 |
| 0 | 0 | 0 | 0 | 0 |

Petit et al., *Environ. Modelling Software*, 2017
https://sites.google.com/site/zefirproject

# PSCF and CF example

**PSCF**

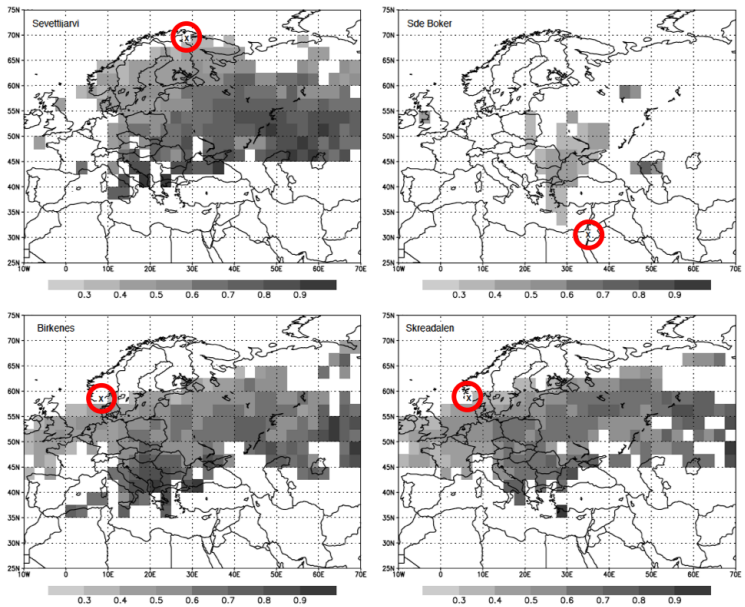


Fig. 3. PSCF bootstrapped spatial distribution of fine sulphur at 95% confidence level, with 75th percentile of the concentration distribution as threshold, for Sevettijärvi, Sde Boker, Birkenes, and Skreådalen. The location of the sites is indicated with an 'x'.

**CF**

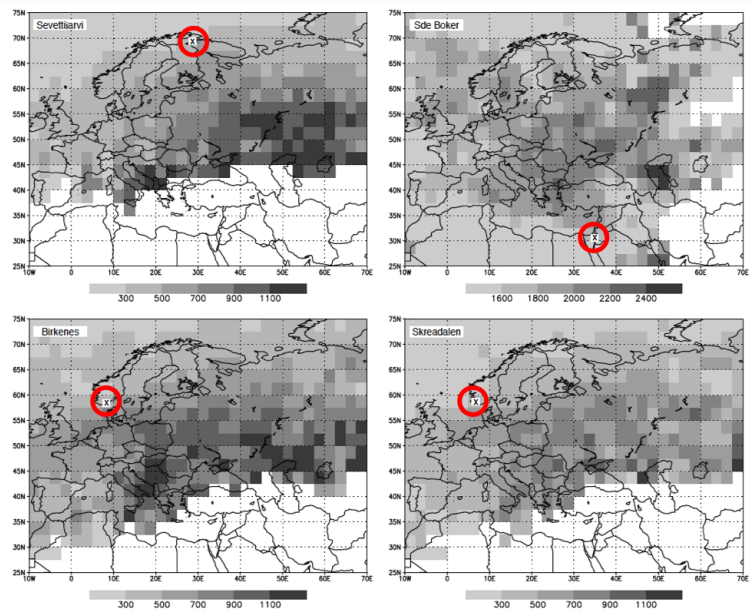


Fig. 2. Fine sulphur concentration field (ng/m$^3$) as computed using CF method for Sevettijärvi, Sde Boker, Birkenes, and Skreådalen. The location of the sites is indicated with an 'x'.

Lupu and Maenhaut, *Atmos. Environ.*, 2002

# Further reading

Topics covered: Atmospheric Dynamics, Boundary Layer, Meteorology, Dispersion Modeling


Arya, P. S. *Introduction to Micrometeorology*. Academic Press, 2001.

Jacob, D. *Introduction to Atmospheric Chemistry*. Princeton University Press, 1999.

Holton, J. R., and Hakim, G. J. *An Introduction to Dynamic Meteorology*. Academic Press, 2012.

Satoh, M. *Atmospheric Circulation Dynamics and General Circulation Models*. Berlin, Heidelberg: Springer Berlin Heidelberg, 2014.

Seinfeld, J. H. & Pandis, S. N. *Atmospheric Chemistry and Physics: From Air Pollution to Climate Change*. John Wiley & Sons, New York, 2006.

Wark, K., Cecil F. W., and Wayne T. D. *Air Pollution: Its Origin and Control*. Addison-Wesley, 3rd ed., 1998.

Vallis, G. K. *Atmospheric and Oceanic Fluid Dynamics: Fundamentals and Large-Scale Circulation*. Cambridge University Press, 2006.

Wallace, J. M., and Hobbs, P. V.. *Atmospheric Science: An Introductory Survey*. Academic Press, 2006.